Experimental Realization of Decoherence-Free Subspace in Neutron Interferometry

Experimental Realization of Decoherence-Free Subspace in Neutron Interferometry

D. A. Pushin,[1,*] M. G. Huber,[2] M. Arif,[2] and D. G. Cory[1,3,4]

[1]*Department of Nuclear Science and Engineering, Massachusetts Institute of Technology, Cambridge, Massachusetts 02139, USA*
[2]*National Institute of Standards and Technology, Gaithersburg, Maryland 20899, USA*
[3]*Perimeter Institute for Theoretical Physics, Waterloo, Ontario, Canada*
[4]*Institute for Quantum Computing and Department of Chemistry, University of Waterloo, Ontario, Canada*

(Received 9 August 2010; published 6 October 2011)

A decoherence-free subspace (DFS) is an important class of quantum-error-correcting (QEC) codes that have been proposed for fault-tolerant quantum computation. The applications of QEC techniques, however, are not limited to quantum-information processing (QIP). Here we demonstrate how QEC codes may be used to improve experimental designs of quantum devices to achieve noise suppression. In particular, neutron interferometry is used as a test bed to show the potential for adding quantum error correction to quantum measurements. We built a five-blade neutron interferometer that incorporates both a standard Mach-Zender configuration and a configuration based on a DFS. Experiments verify that the DFS interferometer is protected against low-frequency mechanical vibrations. We anticipate these improvements will increase the range of applications for matter-wave interferometry.

DOI: 10.1103/PhysRevLett.107.150401 PACS numbers: 03.75.Dg, 03.65.−w, 03.67.Pp, 42.50.−p

A major challenge in the development of quantum computers [1,2] and quantum devices is combatting noise, which dephases or decoherences the quantum state and causes it to become classical [3]. Fortunately, the ideas of quantum error correction [4] have shown us how to protect fragile quantum information by encoding into a larger Hilbert space [5]. With a decoherence-free subspace (DFS) the information is passively protected against noise with a certain symmetry without requiring additional resources [6]

QEC codes have been experimentally demonstrated on several systems [7], but their relevance to experimental design has not yet been fully appreciated. We have previously suggested that a QEC code may be used to design a matter-wave interferometer robust to the dominant noise source, which affects the device quality [8]. Here we demonstrate the realization of such neutron interferometer, which uses a DFS to suppress errors induced by low-freqeuncy mechanical vibrations. The required symmetry arises from the noise being a common mode vibration of the entire interferometer.

Matter-wave interferometers are important tools in the understanding of quantum mechanics [9], but are susceptible to environmental noise due to the slow velocities of matter waves. When describing the phase of the particle inside the interferometer by a classical action along different interferometer paths, we must account for the motion of the device. While traversing a standard Mach-Zender (MZ) interferometer, a particle's momentum and path length will be modified depending on the velocity of the interferometer, causing a relative phase to develop between the two paths. By labeling the paths, mechanical vibrations distinguish between them and destroy the quantum coherence of the device. This leads to a loss of contrast—a measure of the quality of the device related to the amount of coherence between the two paths. The DFS version of the MZ design compensates for the change in relative phase between the two paths, causing the noise to act unitarily on these two paths. The interferometer, then, becomes decoupled from low-frequency vibrations. The immediate consequence of this work is that the DFS interferometer eliminates the need for large vibration isolation systems, making the device more compact and accessible to research in fields such as condensed matter, biology, and spintronics.

We demonstrate the improvements offered by the DFS design by machining a five-blade single crystal neutron interferometer that incorporates both the MZ [10,11] and DFS [8] interferometers in one crystal. The switch between designs occurs *in situ* by moving cadmium (Cd) beam blocks. In Fig. 1(a) we show a drawing of the five-blade interferometer used in this study. It was cut from a crystal Si ingot at the University of Missouri machine shop. The interferometer blades are oriented perpendicular to the (220) crystal planes. The incoming neutron beam coherently splits at these blades by Bragg scattering. To preserve crystallographic registration of the blades, each blade remains attached to the common base.

As shown in Fig. 1, the neutron beam enters the single crystal interferometer from the left and is split coherently by the first blade over two paths. Blades 2, 3, and 4 direct the beams through four different paths and recombine them at the last (fifth) blade. Interference of these paths is observed by ^{3}He detectors placed in the O and H beams. Using Cd blocks we can selectively absorb all neutrons in a given path. As shown in Fig. 1(b), by placing Cd blocks we

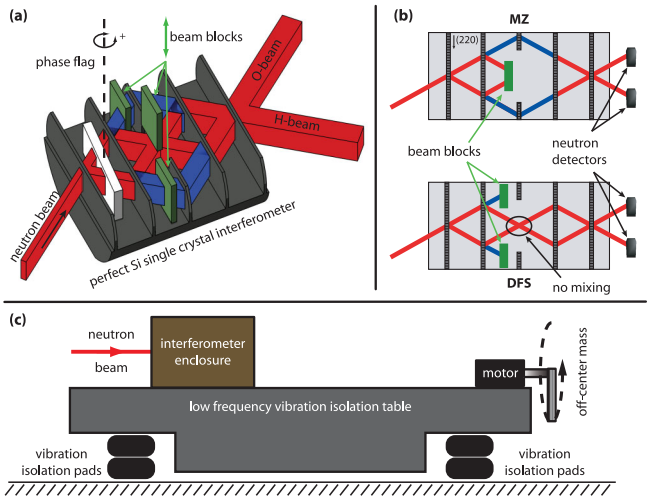

FIG. 1 (color). (a) A diagram of the five-blade neutron interferometer. The neutron beam enters from the left and is coherently split by the first blade via Bragg diffraction, is diffracted by the following sequence of blades, and finally recombined and interferes at the fifth blade. After passing through the interferometer, the beam is captured by ^{3}He detectors in the O and H beams. By moving cadmium shields up or down we can *in situ* select the three (MZ) or four (DFS) blade interferometer configuration. (b) A schematic top-view representation of the five-blade beam paths. The upper diagram represents the MZ setup. Here the beam block removes the two central beam paths and leaves the outer paths untouched. When we block the outer paths only we have the four-blade (DFS) setup, as shown in the lower diagram. (c) A schematic diagram of the neutron interferometer facilities at the National Institute of Standards and Technology. This facility has several vibration isolation stages to remove vibrations above 1 Hz. The primary stage consists of a 40-ton table that floats on actively controlled vibration isolation pads. The interferometer is enclosed in a temperature-controlled box. To test the robustness of the interferometers to mechanical vibrations we introduced vibrations by a motor with an off-center mass attached to the table.

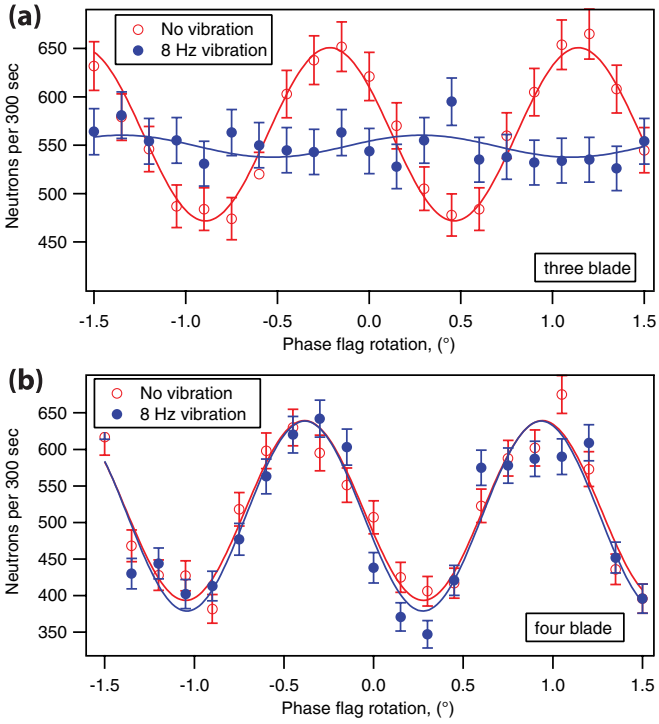

FIG. 2 (color online). (a) Interferograms from the three-blade (MZ) interferometer without vibrations (open circles) and with 8 Hz vibrations (closed circles). We observe a complete loss of contrast with 8 Hz vibrations. (b) Interferograms from the four-blade (DFS) setup at the same conditions as in (a). Within experimental errors there is no loss of contrast from the added vibrations.

can choose either the MZ (three blade, upper schematic diagram) or DFS (four blade, lower diagram) setups.

Figure 1(c) outlines the experimental setup of the Neutron Interferometer and Optic Facilities at the National Institute of Standards and Technology, Gaithersburg, MD. The interferometer is placed inside an enclosure with temperature stability of a few mK to maintain phase stability [12]. The enclosure is isolated from external vibrations by a high position stability ($< 1\ \mu$m) vibration isolation system. A detailed description of this facility can be found in [13]. We add controlled vibrations to the system through a motor with an off-center shaft. We used different lengths and masses to create vibrations with controlled amplitudes. Vibrations were monitored by a short-period seismometer.

To measure the contrast we introduce a phase difference between the two interferometer paths and measure the phase dependence on the output intensity at both the O and H beams. It is convenient to introduce this phase difference through a fused silica phase flag placed between the first and the second blades [see Fig. 1(a)]. Figure 2(a) shows the intensity dependence for the three-blade (MZ) configuration with and without added noise. The vibrations were artificially introduced with a fundamental frequency of 8 Hz. Without vibrations the interferometer has a 12% contrast; with vibrations there is no detectable contrast.

Figure 2(b) shows the contrast for the four-blade (DFS) interferometer under the same conditions used for the three-blade MZ setup. Here there is no measurable loss of contrast with added noise. The contrast in both cases is 23%. As expected, the DFS configuration is more robust to applied noise than the MZ configuration. While the contrasts without vibrations for both the MZ and DFS setups are lower than that seen for the best available neutron interferometers (around 90% [14]), the key fact is the reduced sensitivity to external noise. The reason for the lower contrast is the incoming neutron beam occupies a cross-sectional area of 1×6 mm^2 and blade imperfections lead to a dispersion of phases over this area. With the thin blades in this interferometer we cannot further etch the surface to improve contrast while maintaining proper blade separation. However, this defect is correctable and will be addressed in future implementations of DFS interferometers.

The measured and expected frequency dependence of the contrast of these two (MZ and DFS) setups is shown in Fig. 3. Over the frequency range that requires large vibration isolation systems (typically 5–10 Hz), we see a clear difference between the two. The dominant error that leads to a loss of contrast in the MZ interferometer is the change in neutron momentum due to interaction with a moving blade. At low frequencies the single crystal interferometer moves as a solid body, and both translational and rotational vibrations can result in a distribution of the neutron's momentum. For the MZ configuration, these changes in the neutron's momentum distinguish the paths and lead to a loss of contrast. In the DFS geometry the second reflection avoids the labeling of paths by the neutron's momentum and contrast is restored. Because the interferometer blades vibrate together, reflections at a latter blade can compensate the change in momenta introduced by an earlier blade. A second mechanism leading to a loss in contrast is a defocusing of the neutron path at the last (interfering) blade, from vibrations in the plane of the neutron beam paths and perpendicular to the Bragg vector (x vibrations of [8]). The precision with which the interfering beams must overlap at the final blade to preserve coherence is often described by a coherence length, bound by the inverse of the spread in neutron momenta. Vibrations increase the spread in momenta, thereby decreasing the effective coherence length and leading to lost contrast. The coherence length of the DFS design is insensitive to these vibrations.

As shown before [8], a standard (MZ) neutron interferometer is most sensitive to rotational vibrations while the DFS design is protected from them. The loss of contrast again results from the phase difference between the two paths introduced by the rotational motion. If we describe rotational vibrations as a time-varying angle $\theta(t)$ about the interferometer center of mass, then for the MZ and DFS configurations this phase difference is, respectively (see Supplemental Material [15]),

$$\Delta\Phi_{\mathrm{MZ}} \approx -\frac{8m_nL^2}{\hbar v_{n\perp\mathrm{Bragg}}}[v_{n\|\mathrm{Bragg}} - L\dot{\theta}(0)]\dot{\theta}(0), \quad (1)$$

$$\Delta\Phi_{\mathrm{DFS}} \approx \frac{48m_nL^3}{\hbar v^2_{n\perp\mathrm{Bragg}}}[v_{n\|\mathrm{Bragg}} - 2L\dot{\theta}(0)]\ddot{\theta}(0). \quad (2)$$

Where L is the distance between the interferometer blades, m_n is the neutron mass, and $v_{n\|\mathrm{Bragg}}$ ($v_{n\perp\mathrm{Bragg}}$) is the neutron velocity parallel to (perpendicular to) the Bragg vector. Note that the DFS phase is proportional to the second derivative of the rotation angle while the MZ phase is proportional to the first derivative (compare with y vibrations of [8]). Also, note that for any constant rotation $\theta(t) = \omega t$, thus $\dot{\theta} = \omega$ and $\ddot{\theta} = 0$. The phase difference for the MZ interferometer is then $\Delta\Phi_{\mathrm{MZ}} \propto \omega A$, while the DFS phase difference is zero. A is the area enclosed by the neutron paths of the interferometer.

The same conclusion may be reached by attributing the loss of contrast to the Sagnac effect [16,17]. The Sagnac effect is concerned with the phase introduced in a MZ interferometer by a uniform rotation of the entire interferometer. For a rotating MZ neutron interferometer the Sagnac phase shift is $\Delta\Phi = (2k/v_n)\boldsymbol{\omega}\boldsymbol{A}$, where k is the wave number of the neutron and $\boldsymbol{A}$ is the normal area of the enclosed neutron beam paths. For the DFS design the phase shift will be zero, as noted in [18]. The Sagnac effect is a good model for the protection offered by the DFS interferometer since the time a neutron spends in the interferometer is less than the period of rotational vibrations. So each neutron sees a fixed frequency and the loss of contrast is the result of averaging over many events.

The inset of Fig. 3 shows a numerical simulation of rotational vibrations for both the MZ and DFS interferometers. A detailed description of the model and predictions for different vibrational modes is discussed in [8]. Here we show the expected contrast for six microradian rotational vibrations around the center of mass of the interferometer with a constant amplitude of vibration. In comparison with the MZ setup, the DFS setup preserves the contrast up to higher frequencies. This is confirmed by our experimental data (Fig. 3). For the DFS configuration the contrast eventually falls off, but at such high frequencies that it is easy to avoid in experiments.

Because mirrors do not exist for thermal neutrons, the addition of a second central blade leads to a loss of half the neutron intensity. However, even with this loss, we realize more than an order of magnitude overall increase in neutron intensity by taking advantage of the robust the DFS configuration.

The results of this work offer an example of how advances in quantum-information theory may be applied to experimental design. These results validate our expectation that QEC codes may be used to control the effects of noise

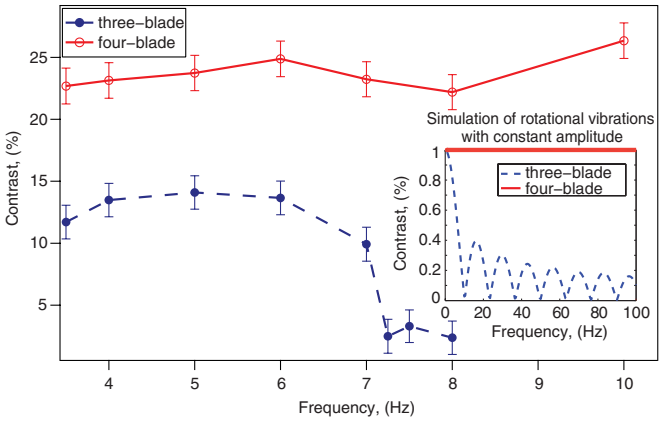

FIG. 3 (color online). Frequency dependence of the contrast with added mechanical vibrations. The dotted line with closed circles is for the three-blade (MZ) setup and straight line with open circles is for the four-blade (DFS) measurements. The inset shows a simulation for rotational vibrations.

on useful macroscopic quantum devices. The use of DFS significantly improves coherent control in neutron interferometry. We anticipate this approach enabling a new series of compact neutron interferometers tailored to specific applications. The techniques demonstrated in this Letter should also be applicable to other systems [19,20] that experience similar noise processes. For example, the effects of undesired center of mass motion caused by common mode mechanical vibrations of beam splitters in Bose-Einstein condensate (BEC) type [21–23], atom, and molecular [24,25] interferometers, should be suppressed by these methods.

This work was supported in part by the National Security Agency (NSA) under Army Research Office (ARO) Contract No. W911NF-05-1-0469, and by the Canada Excellence Research Chairs program. Support from NIST is also gratefully acknowledged. Research was performed in part at the NIST Center for Nanoscale Science and Technology. The authors are grateful to Sam Potts and University of Missouri-Columbia Physics machine shop for machining the interferometer, and for discussions with C. W. Clark, D. L. Jacobson, T. Borneman, R. A. Barankov, P. Cappellaro, E. R. Sparks, and G. L. Greene.

*mitja@mit.edu

[1] C. H. Bennett and D. P. DiVincenzo, Nature (London) **404**, 247 (2000).
[2] D. DiVincenzo, Fortschr. Phys. **48**, 771 (2000).
[3] A. J. Leggett, S. Chakravarty, A. T. Dorsey, M. P. A. Fisher, A. Garg, and W. Zwerger, Rev. Mod. Phys. **59**, 1 (1987); W. H. Zurek, Rev. Mod. Phys. **75**, 715 (2003).
[4] J. Preskill, Proc. R. Soc. A **454**, 385 (1998).
[5] P. Zanardi, Phys. Rev. A **63**, 040304 (2001).
[6] D. A. Lidar, I. L. Chuang, and K. B. Whaley, Phys. Rev. Lett. **81**, 2594 (1998); P. Zanardi and M. Rasetti, Phys. Rev. Lett. **79**, 3306 (1997); L.-M. Duan and G.-C. Guo, Phys. Rev. Lett. **79**, 1953 (1997); E. Knill, R. Laflamme, and L. Viola, Phys. Rev. Lett. **84**, 2525 (2000); L. Viola, E. M. Fortunato, M. A. Pravia, E. Knill, R. Laflamme, and D. G. Cory, Science **293**, 2059 (2001).
[7] D. G. Cory, M. D. Price, W. Maas, E. Knill, R. Laflamme, W. H. Zurek, T. F. Havel, and S. S. Somaroo, Phys. Rev. Lett. **81**, 2152 (1998); P. Kwiat, A. Berglund, J. Altepeter, and A. White, Science **290**, 498 (2000); D. Kielpinski, V. Meyer, M. Rowe, C. Sackett, W. Itano, C. Monroe, and D. Wineland, Science **291**, 1013 (2001).
[8] D. A. Pushin, M. Arif, and D. G. Cory, Phys. Rev. A **79**, 053635 (2009).
[9] A. J. Leggett, *The Lessons of Quantum Theory*, edited by J. de Boer, E. Dal, and O. Ulfbeck (Elsevier, Amsterdam, 1986).
[10] H. Rauch, W. Treimer, and U. Bonse, Phys. Lett. A **47**, 369 (1974).
[11] W. Bauspiess, U. Bonse, H. Rauch, and W. Treimer, Z. Phys. **271**, 177 (1974).
[12] D. A. Pushin, M. Arif, M. G. Huber, and D. G. Cory, Phys. Rev. Lett. **100**, 250404 (2008).
[13] M. Arif, D. E. Brown, G. L. Greene, R. Clothier, and K. Littrell, Proc. SPIE Int. Soc. Opt. Eng. **2264**, 20 (1994).
[14] H. Rauch and S. A. Werner, *Neutron Interferometry* (Oxford University Press, New York, 2000).
[15] See Supplemental Material at http://link.aps.org/supplemental/10.1103/PhysRevLett.107.150401 for a more detailed description of this derivation and also Kraus representation of decoherence induced by mechanical vibration.
[16] G. Sagnac, C. R. Hebd. Seances Acad. Sci. **157**, 708 (1913); A. Michelson, H. Gale, and F. Pearson, Astrophys. J. **61**, 140 (1925).
[17] S. A. Werner, J. L. Staudenmann, and R. Colella, Phys. Rev. Lett. **42**, 1103 (1979).
[18] B. Mashhoon, Phys. Rev. Lett. **61**, 2639 (1988); J. F. Clauser, Physica (Amsterdam) **151B+C**, 262 (1988).
[19] *Atom Interferometry*, edited by P. R. Berman (Academic Press, San Diego, 1997).
[20] A. D. Cronin, J. Schmiedmayer, and D. E. Pritchard, Rev. Mod. Phys. **81**, 1051 (2009).
[21] Y. Torii, Y. Suzuki, M. Kozuma, T. Sugiura, T. Kuga, L. Deng, and E. W. Hagley, Phys. Rev. A **61**, 041602 (2000).
[22] J. Denschlag, J. E. Simsarian, D. L. Feder, C. W. Clark, L. A. Collins, J. Cubizolles, L. Deng, E. W. Hagley, K. Helmerson, and W. P. Reinhardt, Science **287**, 97 (2000).
[23] S. Gupta, K. Dieckmann, Z. Hadzibabic, and D. E. Pritchard, Phys. Rev. Lett. **89**, 140401 (2002).
[24] D. W. Keith, M. L. Schattenburg, H. I. Smith, and D. E. Pritchard, Phys. Rev. Lett. **61**, 1580 (1988).
[25] E. M. Rasel, M. K. Oberthaler, H. Batelaan, J. Schmiedmayer, and A. Zeilinger, Phys. Rev. Lett. **75**, 2633 (1995).